Electric Field Alignment of Asymmetric Diblock Copolymer Thin Films

T. Xu,[†] A. V. Zvelindovsky,[‡] G. J. A. Sevink,[§] K. S. Lyakhova,[§] H. Jinnai,[⊥] and T. P. Russell*,[†]

Department of Polymer Science and Engineering, University of Massachusetts, Amherst, Massachusetts 01003, Centre for Materials Science, Department of Physics, Astronomy & Mathematics, University of Central Lancashire, Preston, PR1 2HE, United Kingdom, Leiden Institute of Chemistry, Leiden University, P.O.Box 9502, 2300 RA Leiden, The Netherlands, and Department of Polymer Science and Technology, Kyoto Institute of Technology, Kyoto 606-8585, Japan

Received March 10, 2005; Revised Manuscript Received September 14, 2005

ABSTRACT: The electric field alignment of cylindrical microdomains in diblock copolymer thin films was studied using small-angle neutron scattering and transmission electron microscopy. The alignment process was followed with the block copolymer films in different initial states. Starting from a poorly ordered state, the cylindrical microdomain orientation was biased by the surface field that initially drove the cylindrical microdomains to be oriented parallel to the film surface. With further annealing, the cylinders were disrupted locally and formed ellipsoid-shaped microdomains that, with time, connected into cylindrical microdomains oriented in the field direction. Starting from an ordered state with cylinders parallel to the surface, the applied electric field enhanced fluctuations at the interfaces of the microdomains. The growth of the fluctuations continued until the cylindrical microdomains broke up into spherical microdomains, similar to that seen in the thermoreversible cylinder-to-sphere order−order transition. With time, the spherical microdomains deformed into ellipsoidal domains that reconnected into cylindrical microdomains oriented at ∼45° with respect to the applied field direction. Further annealing aligned the tilted cylinders along the applied field direction. This reorientation process was much slower than from the poorly ordered state. The details of the realignment process are supported by computer simulations based on dynamic self-consistent-field theory.

Introduction

Block copolymer thin films have significant potential as templates and scaffolds for the fabrication of arrays of nanometer-scale structures.[1−3] The microdomains are typically oriented parallel to the surface due to the preferential wetting of one block with the surface.[4−7] Electric fields, however, have proven to be an effective means to align the microdomains.[3,8−11] For example, cylindrical microdomains in thin films of diblock copolymers of polystyrene-*b*-poly(methyl methacrylate) can be oriented normal to the substrate using an electric field.[3,10,12,13] Subsequently, nanoporous films can be made by the selective removal of the minor component comprising the cylindrical microdomains.[3,12] The pore size can be easily tuned by varying the molecular weight of the copolymer.[13]

Electric field alignment of lamellar and cylindrical microdomains in diblock copolymers has been studied in the bulk and in thin films.[3,8−11,14−28] Amundson suggested that, starting from a disordered state, the final oriented morphology is obtained by a simultaneous orientation and ordering of the lamellar microdomains, whereas, starting from randomly oriented lamellar microdomains, alignment occurs by movement of grain boundaries, such that regions of favorable orientation grow at the expense of others.[8,14,15] Krausch and coworkers[20] and Zvelindovsky et al.[28] found that, with ordered lamellar microdomains in concentrated copolymer solutions, whether orientation occurs via grain boundary migration or grain rotation is determined by the magnitude of the interactions between two blocks.[20,28] Thurn-Albrecht et al. followed the alignment process of cylindrical microdomains using in-situ small-angle X-ray scattering and found that the pathway depended upon the initial state. From the disordered melt, the applied field biases concentration fluctuations that template the formation of an oriented microphase-separated morphology. They assumed that the orientation of the copolymer obtained after spin-coating would occur by a similar route. For a copolymer having ordered microdomains normal to the field direction, the applied field leads to an instability that enables the large grains in the initial copolymer to be broken up into smaller sections. However, the wavelength of this instability was not determined experimentally.[22] Recently, our transmission electron microscopy study on the electric field alignment of lamellar microdomains in thin films showed that the applied electric field enhanced fluctuations at the interfaces of the microdomains with a wavelength comparable to L_0, the equilibrium period of the copolymer. The enhancement in the fluctuations led to a disruption of the microdomains into sections $\sim L_0$ in size that, with time, reconnected to form microdomains oriented in the direction of the applied field.[26,27]

A full understanding of the alignment process in thin films beginning from different initial states is important for efficiently preparing films suitable for subsequent applications. Most studies have been performed by scattering methods on films that were 20−50 μm in thickness. For many applications, copolymer thin films having cylindrical microdomains with thicknesses less than 1 μm are desirable. Interfacial interactions become increasingly important with decreasing film thickness, and grain rotation is precluded due to the confining geometry presented by film thickness. From transmis-

[†] University of Massachusetts.
[‡] University of Central Lancashire.
[§] Leiden University.
[⊥] Kyoto Institute of Technology.

10.1021/ma050521c CCC: $30.25
Published on Web 11/19/2005

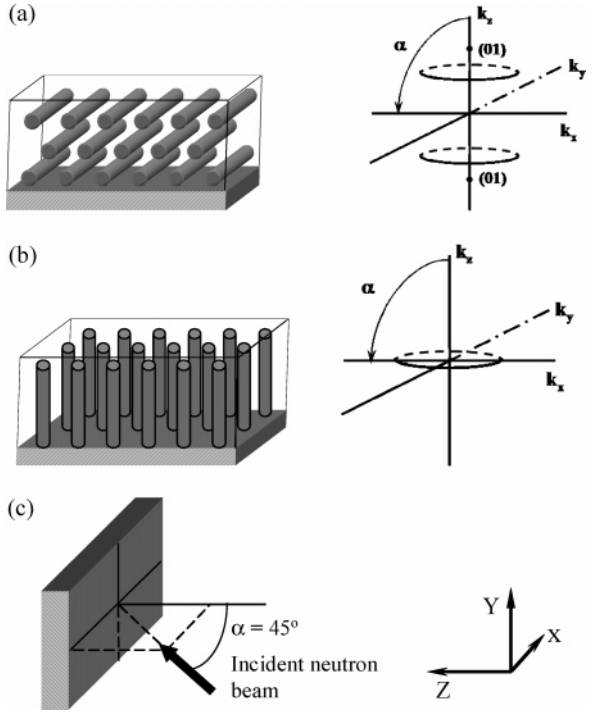

Figure 1. Schematic diagram of hexagonally packed cylinders (a) parallel and (b) perpendicular to the surface in the real and reciprocal space. (c) The geometry of SANS measurement.

sion electron microscopy and small-angle scattering studies, information in both real space and reciprocal space can be obtained to address the alignment process quantitatively. In particular, the length scale of the fluctuations, the effect of interfacial interactions, and the formation of defects can be studied.

Here, the electric field alignment of cylindrical microdomains in diblock copolymer thin films of polystyrene-*block*-poly(methyl methacrylate), PS-*b*-PMMA, was investigated using small-angle neutron scattering (SANS) and transmission electron microscopy (TEM). Thin films of PS-*b*-PMMA with different initial states were studied. In one case, films were annealed under an applied electric field after spin-coating (as cast), i.e., starting from a poorly ordered state. In the second case, films were preannealed so that the majority of the cylindrical microdomains were oriented parallel to the substrate. In both cases, the electric field alignment process is seen to be a competition between interfacial interactions and the applied electric field. Initially, at the copolymer/substrate interface, preferential interactions induce an orientation of the microdomains parallel to the interface, and the applied electric field biases the orientation of the cylindrical microdomain in the center of the film. With further annealing, the copolymers locally rearrange and connect into cylindrical microdomains oriented in the field direction. For copolymer thin films starting from an ordered state with the cylindrical microdomains oriented parallel to the surface, the applied electric field is seen to amplify fluctuations at the interfaces of the microdomains with a wavelength comparable to D, the center-to-center distance of the cylindrical microdomains. Further enhancement of the fluctuations leads to a disruption of the cylindrical microdomains into spherical microdomains. TEM images of this electric-field-induced sphere-to-cylinder transition are very similar to the thermoreversible cylinder-to-sphere transition observed by Lodge and coworkers and Hashimoto and co-workers.[29−32] With time, the spheres deform into ellipsoids and reconnect to form cylindrical microdomains oriented at ∼45° with respect to the applied field. Further annealing aligns the cylinders parallel to the applied field direction. The growth of fluctuations and formation of the spherical microdomains increase the interfacial area between the copolymer microdomains which presents a high energetic barrier to this reorientation process. Consequently, the time scale for alignment of an ordered film is much longer than for a film beginning from a poorly ordered state.

Experimental Section

Asymmetric diblock copolymers of PS-*b*-PMMA with a number-average molecular weight of 1.2×10^5 g/mol (120K) and a PS volume fraction of 0.72 with a polydispersity of 1.05 were synthesized anionically. SANS studies were performed with PS-*b*-PMMA where the polystyrene block was deuterated, denoted as dPS-*b*-PMMA. The molecular weight of dPS-*b*-PMMA was 4.7×10^4 g/mol (47K) with a polydispersity of 1.04 and a dPS volume fraction of 0.7. The center-to-center distance, $D = 4\pi/\sqrt{3}q_{10}$, between cylindrical microdomains of dPS-*b*-PMMA (47K) is ∼32 nm, corresponding to a scattering vector $q_{10} = 0.22$ nm^{-1}. Here, $q_{10} = 4\pi/\lambda \sin\theta$, where λ is the neutron wavelength and 2θ is the scattering angle. Films, 200−700 nm in thickness, were prepared by spin-coating a toluene solution of the copolymer onto a silicon substrate. The silicon substrate was modified with a random copolymer of styrene and methyl methacrylate having a 0.7 volume fraction of styrene. Consequently, the modified substrate has a slightly lower interfacial energy or interaction with PS ($\gamma_{PMMA/sub} - \gamma_{PS/sub} \approx 0.45$ dyn/cm).[33] Thin films of the copolymer were heated to 170 °C for 72 h under vacuum.

In the electric field experiments, an aluminized Kapton film was used as the upper electrode, where a thin (20−25 μm) layer of cross-linked poly(dimethylsiloxane) (PDMS) (Sylgard) was used as a buffer layer between the Kapton electrode and the copolymer thin film so as to remove any air gaps between the electrode and the surface of the copolymer. The preparation of the cross-linked PDMS layer has been described previously. Thin films of dPS-*b*-PMMA (47K) were annealed at 170 °C under an applied electric field of ∼40 V/μm for a predetermined period of time and quenched to room temperature without removing the applied field. A small portion of the sample was removed for TEM studies. After the SANS measurements, the sample was returned to an oven preheated to 170 °C under an applied electric field. Transmission SANS experiments were performed on beamline NG-3, a 30 m SANS instrument at the National Institute of Standard and Technology (NIST), using neutrons with a wavelength $\lambda = 0.6$ nm and $\Delta\lambda/\lambda = 0.15$. The exposure time for each frame was 15 min. To prepare TEM samples, a thin layer of carbon (10−20 nm) was coated onto the surface before the film was embedded in epoxy and cured at 60 °C for 12 h. The film was removed from the substrate by dipping into liquid N_2, microtomed at room temperature using a diamond knife and transferred to a copper grid. The cutting angle was 90 ± 2° with respect to the substrate (parallel to the electric field direction), as confirmed by optical microscopy. The thin sections were exposed to ruthenium tetraoxide vapor for 15−20 min to enhance the contrast. Electron microscopy experiments were performed on a JEOL 200 kV TEM.

3-D TEM Tomography. TEM tomography was used to investigate the 3-D morphology of PS-*b*-PMMA in the thin films. A tilt series of TEM projections were taken typically from −60° to 60° in 1° increments on a JEOL JEM-2200FS microscope (JEOL, Co. Ltd., Japan) operated at 200 kV. The maximum and minimum tilt angles varied for different samples (details are given in the figure captions). Digitized transmitted images were collected with a slow-scan CCD camera (Gatan USC1000, Gatan Inc.). To obtain achromatic projections, transmitted or elastically scattered electrons

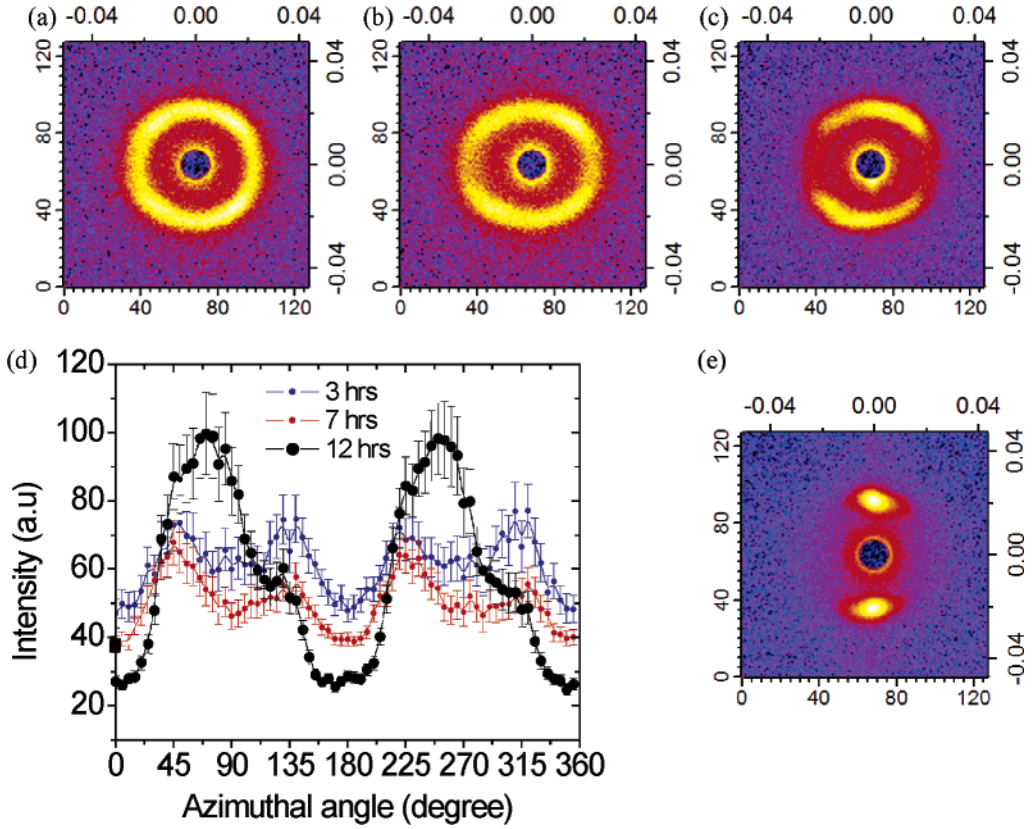

Figure 2. 2-D SANS patterns of a ~500 nm dPS-*b*-PMMA (47K) film annealed at 170 °C under a ~40 V/μm electric field for (a) 3, (b) 7, and (c) 14 h. (d) The integrated peak intensity as a function of azimuthal angle of SANS patterns in (a, b, and c). (e) 2-D SANS pattern of another dPS-*b*-PMMA (47K) film annealed at 170 °C under a ~40 V/μm electric field for 16 h without interruption.

(electron energy loss: 0 ± 15 eV) were selected by an energy filter installed in JEM-2200FS (Omega filter, JEOL Ltd., Japan). Prior to 3-D TEM tomographic observations, 5 nm diameter gold particles were placed on the ultrathin sections using a colloidal gold dispersion (GCN005, BBInternational Ltd., UK). The gold particles were used as fiducial markers for the alignment of the tilt series of the TEM images. The tilt series of the TEM images was carefully aligned by the fiducial marker method and, then, reconstructed on the basis of the filtered-back-projection method.[34,35]

Computer Simulation. A computer simulation was performed to mimic the electric-field-induced alignment of the cylindrical microdomains in thin films. The simulation is based on the dynamic self-consistent-field (DSCF) theory.[36] The time evolution of the system is modeled by diffusion dynamics

$$\partial\rho(\mathbf{r},t)/\partial t = M\nabla^2\mu + \eta \qquad (1)$$

where ρ is the concentration of monomers of one type (defined as number of monomers per volume); it has dimensions of inverse volume. In the case of an incompressible diblock copolymer melt, description with a single concentration of one chosen component is sufficient. The chemical potential for the chosen block type is denoted by μ; it has dimensions of kT. The constant mobility coefficient M and the thermal noise term η are related to each other via the fluctuation−dissipation theorem.[37] The chemical potential in the presence of an electric field $\mathbf{E}(\mathbf{r})$ is[38]

$$\mu = \mu^0 - (\partial\epsilon/\partial\rho)_T E^2/8\pi \quad \text{(in CGS units)} \qquad (2)$$

where μ^0 is the chemical potential in the absence of the electric field, $\epsilon(\mathbf{r})$ is the local dielectric constant of the material, and $E = |\mathbf{E}|$. Since copolymer blocks have different dielectric properties, the local dielectric constant is a function of the local concentration ρ. We expand the dielectric constant around the overall concentration $\bar{\rho}$ (averaged over the sample): $\epsilon(\mathbf{r},t) \approx \bar{\epsilon} + \epsilon_1(\rho(\mathbf{r},t) - \bar{\rho})$. The coefficients $\bar{\epsilon}$ and $\epsilon_1$are defined as follows: $\bar{\epsilon} \equiv \epsilon|_{\rho=\bar{\rho}}$ and $\epsilon_1 \equiv (\partial\epsilon/\partial\rho)_{\rho=\bar{\rho}}$. Note that, since ρ has the dimensions of inverse volume, $\bar{\epsilon}$ and ϵ_1 are of different dimensions. The electric field inside the material can be expressed via an auxiliary potential φ: $\mathbf{E} = \mathbf{E}_0 - \nabla\varphi$, where $\mathbf{E}_0 = (0,0,E_0)$ is the uniformly applied electric field along the z-axis. Then the contribution to the chemical potential due to the presence of an electric field, eq 2, can be determined from $\mu^{el} \approx -\epsilon_1(E_0^2 - 2E_0\nabla_z\varphi)/8\pi$. Similarly, the linear expansion of the Maxwell equation div $\epsilon\mathbf{E} = 0$ gives $\bar{\epsilon}\nabla^2\varphi = \epsilon_1 E_0\nabla_z\rho$. Substituting the last two expressions into eq 1, we obtain an anisotropic diffusion equation[28]

$$\partial\rho/\partial t = M\nabla^2\mu^0 + \alpha\nabla_z^2\rho + \eta \qquad (3)$$

where $\alpha \equiv M\epsilon_1^2E_0^2/4\pi\bar{\epsilon}$.

It is convenient to introduce dimensionless variables and parameters. The local monomer volume fraction and its average value for a chosen copolymer component are $f = v\rho$ and $\bar{f} = v\bar{\rho}$, respectively, where v is the volume occupied by a single block copolymer molecule. Then, we have $\epsilon_1 \equiv v\epsilon' = v(\partial\epsilon/\partial f)_{f=\bar{f}}$. The dimensionless electric field strength is $\tilde{\alpha} \equiv \alpha/kTMv$, which depends on the square of the electric field. The dimensionless time-step in eq 3 is $\Delta\tau \equiv \Delta tkTMv/h^2$, where h is the numerical grid spacing. The grid spacing h is related to the statistical segment length a of Gaussian chain by $h/a = 0.866$.[37] The time step is set equal to the value 0.5 to ensure stability of the numerical schemes.[37]

The chemical potential μ^0 is calculated using self-consistent-field theory for A_NB_M Gaussian chains confined between two walls.[39] The model system is an A_3B_7 melt, which has a cylindrical microdomain morphology for the Flory−Huggins interaction parameter $\chi_{AB} = 1.9$. The volume fraction of the minority component, 0.3, matches the experimental system. The size of the simulation box is 32 × 32 × 44 (in units of h). Two electrodes at $z = 1$ and $z = 44$ preferentially interact with the longer block ($\chi_{AE} = 2.3$, $\chi_{BE} = 0$) so as to mimic the experimental conditions.

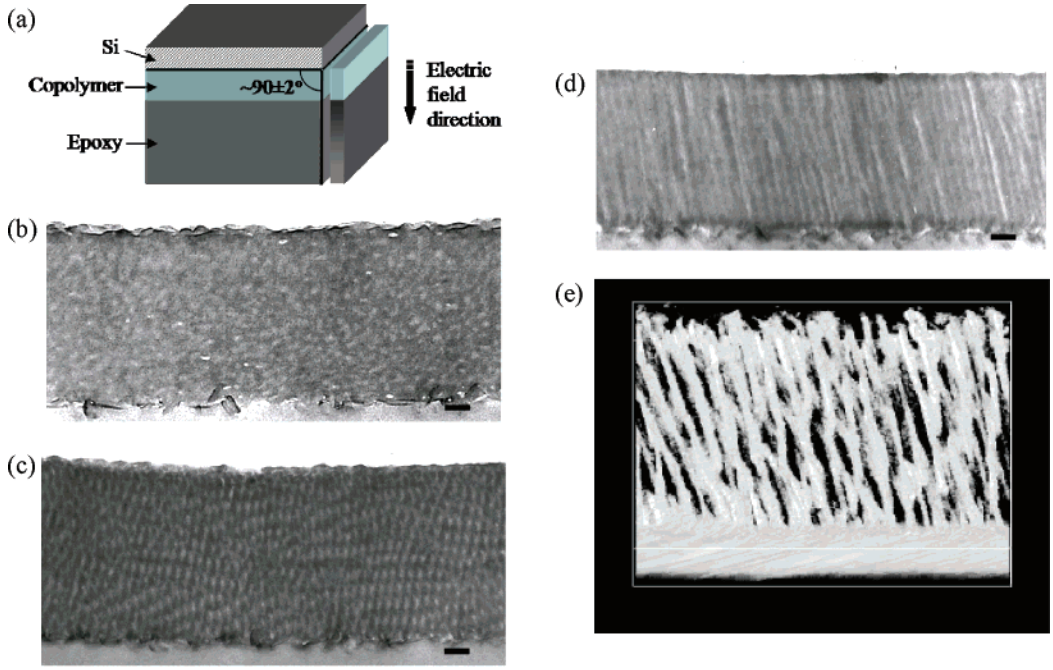

Figure 3. (a) Schematic diagram of TEM sample preparation. Cross-sectional TEM images of ~700 nm PS-*b*-PMMA (120K) films after annealing at 185 ± 5 °C under a ~40 V/μm electric field for (b) 9, (c) 12, and (d) 16 h. Scale bar: 100 nm. (e) A snapshot of PS-*b*-PMMA morphology (3-D TEM tomography of (c)). The box size corresponds to 1029 nm × 740 nm × 236 nm. The top surface corresponds to the copolymer/substrate interface and the bottom to the copolymer/electrode interface. PMMA microdomains appear lighter color due to the lower electron density.

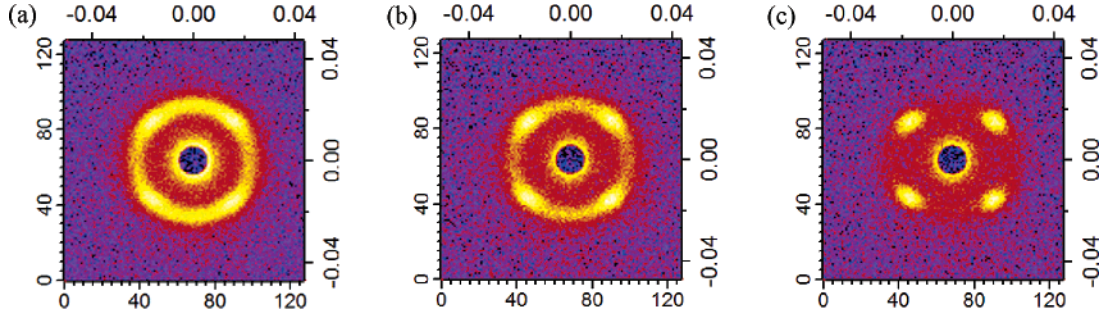

Figure 4. 2-D SANS patterns of (a) ~200, (b) ~300, and (c) ~500 nm dPS-*b*-PMMA (47K) film annealed at 170 °C under vacuum for 72 h.

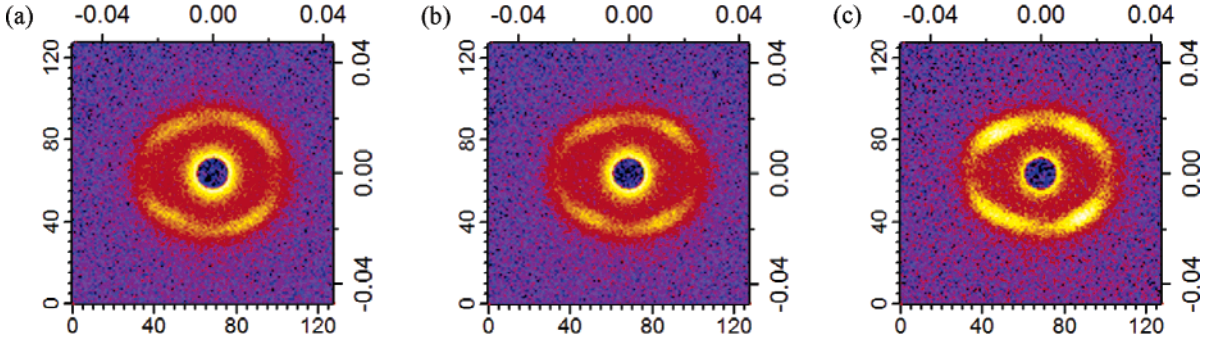

Figure 5. 2-D SANS patterns of a ~300 nm preannealed dPS-*b*-PMMA (47K) film annealed under a ~40 V/μm electric field for (a) 3, (b) 7, and (c) 29 h, respectively.

The purpose of the present simulation is to determine general features of the kinetic pathway of the transition observed experimentally, as opposed to determining exact values of parameters. It is instructive, though, to estimate whether our parameters are in reasonable experimental reach. We consider experimental system PS-*b*-PMMA with molecular weight 120K and PMMA volume fraction $\bar{f} = 0.28$. Using the values for the molecular weight of monomers $M_{PMMA} = 100$ g/mol and $M_{PS} = 104$ g/mol together with polymer densities 1.1 g/cm^3 for PMMA and 1.04 g/cm^3 for PS, one finds the volume occupied by one polymer chain is equal to $v = 266$ nm^3. We assume linear dependency of the dielectric constant on composition: $\epsilon = \epsilon_{PMMA} f + \epsilon_{PS}(1 - f)$, which gives $\bar{\epsilon} = \epsilon_{PMMA}\bar{f} + \epsilon_{PS}(1 - \bar{f})$ and $\epsilon' = \epsilon_{PMMA} - \epsilon_{PS}$. Using the expression in SI units $\tilde{\alpha} = v\epsilon_0\epsilon'^2 E_0^2/kT\bar{\epsilon}$ (where ϵ_0 is the dielectric constant of vacuum) and the dielectric constants of pure components, $\epsilon_{PMMA} = 6$ and $\epsilon_{PS} = 2.5$,[10,21,23] one can find the value of an applied electric field E_0. For the temperature $T = 185$ °C and $\tilde{\alpha} = 0.1$ (the largest value used in the simulation) the electric field is well within experimental range: $E_0 \approx 9$ V/μm.

Using the notation for the diffusion coefficient $D = kTMv$ (the mobility M has dimension of [J m s]$^{-1}$), we get for the

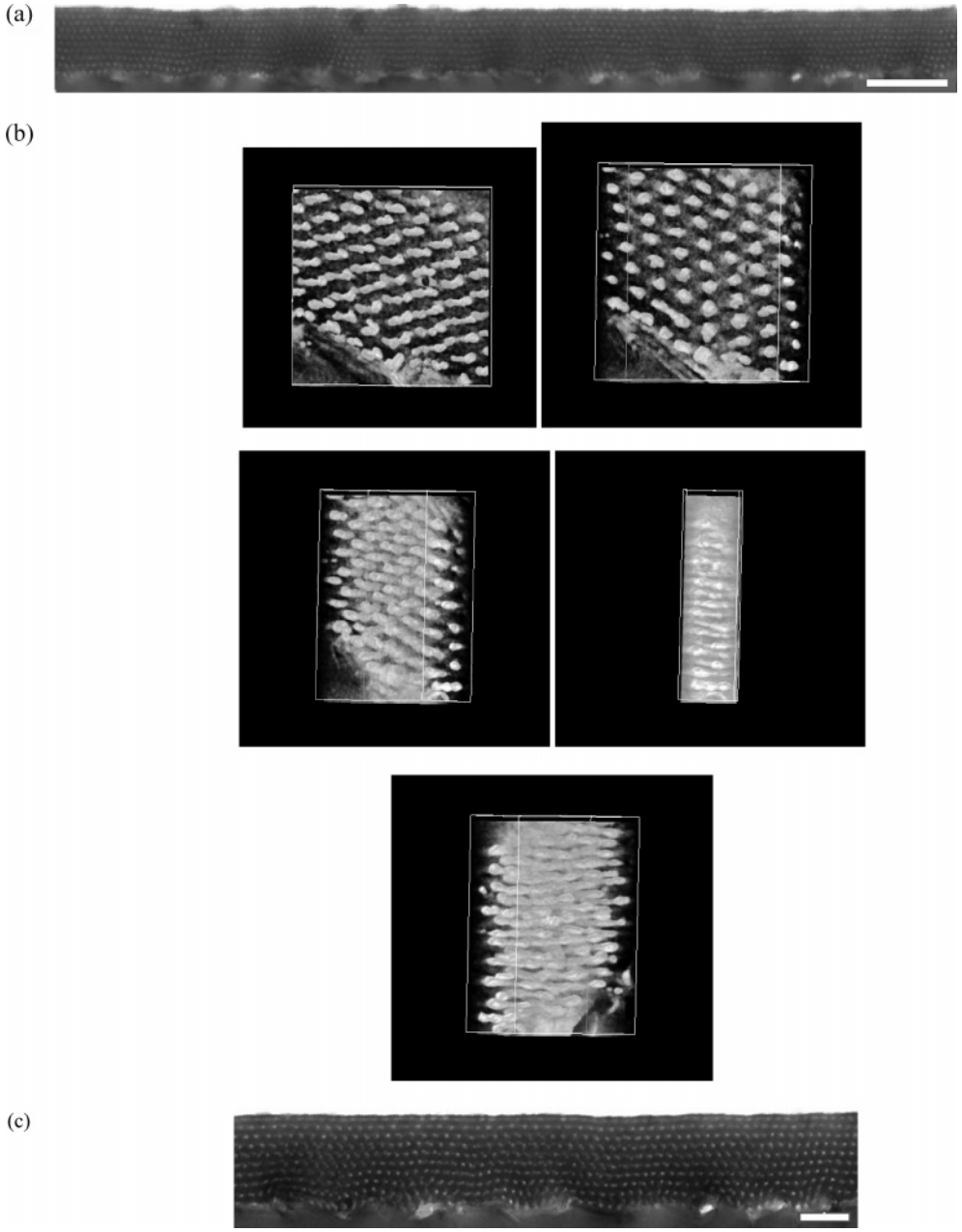

Figure 6. (a) Cross-sectional TEM image of a ~300 nm preannealed dPS-*b*-PMMA (47K) thin film after annealing under a ~40 V/μm electric field for 29 h. Scale bar: 200 nm. (b) 3-D TEM tomography of partial Figure 8a. A series of snapshots of PS-*b*-PMMA morphology (8a) viewing from different angles. The section was tilted from −70° to 63° with 1° increment. The box size is 1290 nm × 940 nm × 100 nm. The top surface corresponds to the copolymer/electrode interface and the bottom to the copolymer/substrate interface. PMMA microdomains appear lighter color due to the lower electron density. (c) Zoom-in image of Figure 8a. Scale bar: 100 nm.

time step introduced above $\Delta t = 0.375a^2/D$. We estimate segment length a from the chain volume $v = N\pi a^3/6$, where $N = 10$ is the number of beads in the model Gaussian chain. For $v = 266$ nm^3 we get $a \approx 3.7$ nm (comparing microdomain spacing would give a more accurate estimate). As the majority component of the experimental block copolymer is PS, this block is the limiting block in the molecular diffusion of PS-*b*-PMMA. Therefore, using data from the literature for the diffusion of hydrogenated PS homopolymer (120K) at 150 °C, $D \approx 10^{-14}$ cm/s,[40] we get $\Delta t \approx 5$ s, which results in about 14 h of physical time for an average simulation of 10^4 time steps.

Results and Discussion

Shown in Figure 1a is a schematic diagram of hexagonally packed cylinders oriented parallel to the film surface in real and reciprocal space. The rings in reciprocal space result from the random orientation of grains in the plane of the film. This corresponds to rotating the scattering pattern around the z-axis. By varying the incidence angle (α) of the neutron beam, defined with respect to the substrate normal ($\alpha = 0$), the observation plane intersects the reciprocal space image or scattering pattern at different points. If the cylinders are oriented normal to the surface, as shown in Figure 1b, the characteristic reflections appear in the k_xk_y plane. Since there are different orientations of the grains of the hexagonally packed cylinders in the plane of the film, a ring of scattering is seen for $\alpha = 0°$. For any other incidence angle, two arcs (or spots) are seen. For an isotropic sample, the scattering pattern consists of a uniform ring independent of the incidence angle.

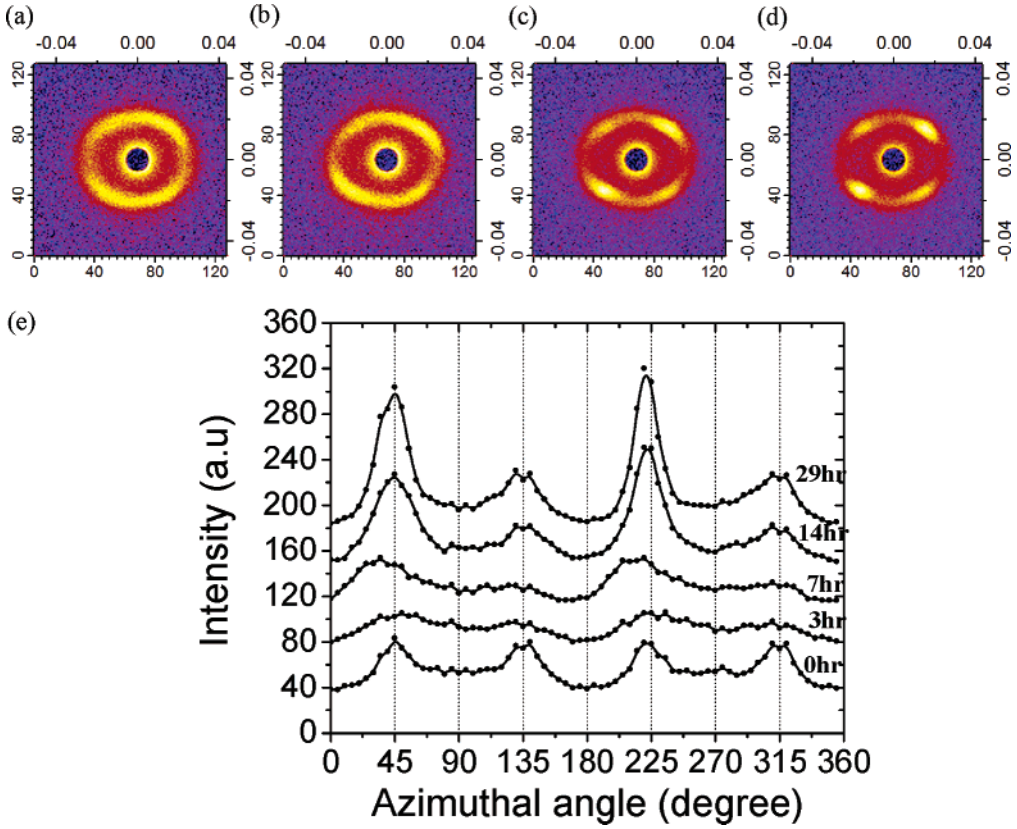

Figure 7. 2-D SANS patterns of a preannealed dPS-*b*-PMMA (47K) film annealed under a ~40 V/μm electric field for (a) 3, (b) 7, (c) 14, and (d) 29 h. (e) The integrated peak intensities as a function of azimuthal angle of SANS patterns in (a, b, c, and d). The plots were shifted 40 units with each other for clarity.

All measurements shown here were taken at $\alpha = 45°$, using the geometry shown in Figure 1c. Thus, a four-point scattering pattern with reflections at 45°, 135°, 225°, and 315° indicates cylinders oriented parallel to the surface, and a two-spot pattern indicates cylinders oriented normal to the surface.

Initial State: Poorly Ordered (As-Cast Thin Films). The alignment of a film beginning in the poorly ordered state was studied using a ~500 nm as-cast dPS-*b*-PMMA (47K) film. The as-cast film was dried to remove residual solvent. The film was annealed at 170 °C under ~40 V/μm electric field for a predetermined time and quenched to room temperature for the SANS measurements. Figure 2a−c shows the 2-D SANS patterns of the film annealed for 3, 7, and 14 h, respectively. In Figure 2a, a ring pattern is seen indicating that the cylindrical microdomains are randomly oriented after a 3 h anneal. Inspection of the integrated peak intensity as a function of azimuthal angle (shown in Figure 2d) shows greater scattering intensities at ~45°, 90°, 135°, 225°, 270°, and 315°. This indicates that the scattering pattern is a superposition of a ring, a two-spot pattern arising from the microdomains oriented normal to the film surface, and a four-spot pattern arising from cylindrical microdomains oriented parallel to the film surface. As shown by Thurn-Albrecht et al.,[10,21] the two-spot pattern originated from the biasing of the concentration fluctuations by the applied field in the center of the film. The four-spot pattern comes from the copolymer microdomains near the interface that are strongly biased by the interface. Initially they orient parallel to the interface.[6] These results show that, in thin films, the orientation of the microdomains is a consequence of a competition between a surface field (interfacial interactions) and the applied electric field. Initially, the surface field dominates.[25−27] With time, as shown in Figure 2b,c, the applied field aligns the microdomains in the field direction. The total scattering (or intensity) seen in Figure 2b is lower than that in Figure 2a, since only a fraction of the microdomains are oriented in a direction that contributes to the scattering at a fixed incidence angle. Parts a−c of Figure 2 were obtained from one sample by annealing the sample for a predetermined time in order to eliminate slight differences between samples that would hamper the elucidation of the mechanism of orientation. After the SANS measurements, the sample, under an applied electric field, was returned to an oven preheated to 170 °C. Because of the difference in thermal expansion coefficients between cross-linked PDMS and Kapton, air bubbles can be trapped between the top electrode and film surface. The presence of air bubbles effectively reduces the electric field strength dramatically to the point where surface fields can dominate or the orientation of the cylindrical microdomains can be slowed down significantly. In either of these cases it will reduce the degree of orientation. Figure 2e shows a 2-D SANS pattern of another ~500 nm film after annealing at 170 °C under a ~40 V/μm applied electric field for 16 h without interruptions. A high degree of orientation is clearly seen.

TEM was used to study the electric field alignment of an as-cast film in real space. A block copolymer with a higher molecular weight (120K vs 45K) was used to obtain clearer images, since the copolymer was poorly ordered initially. Shown in Figure 3b−d are cross-sectional TEM images of ~700 nm as-cast PS-*b*-PMMA (120K) films after annealing at 185 ± 5 °C under ~40

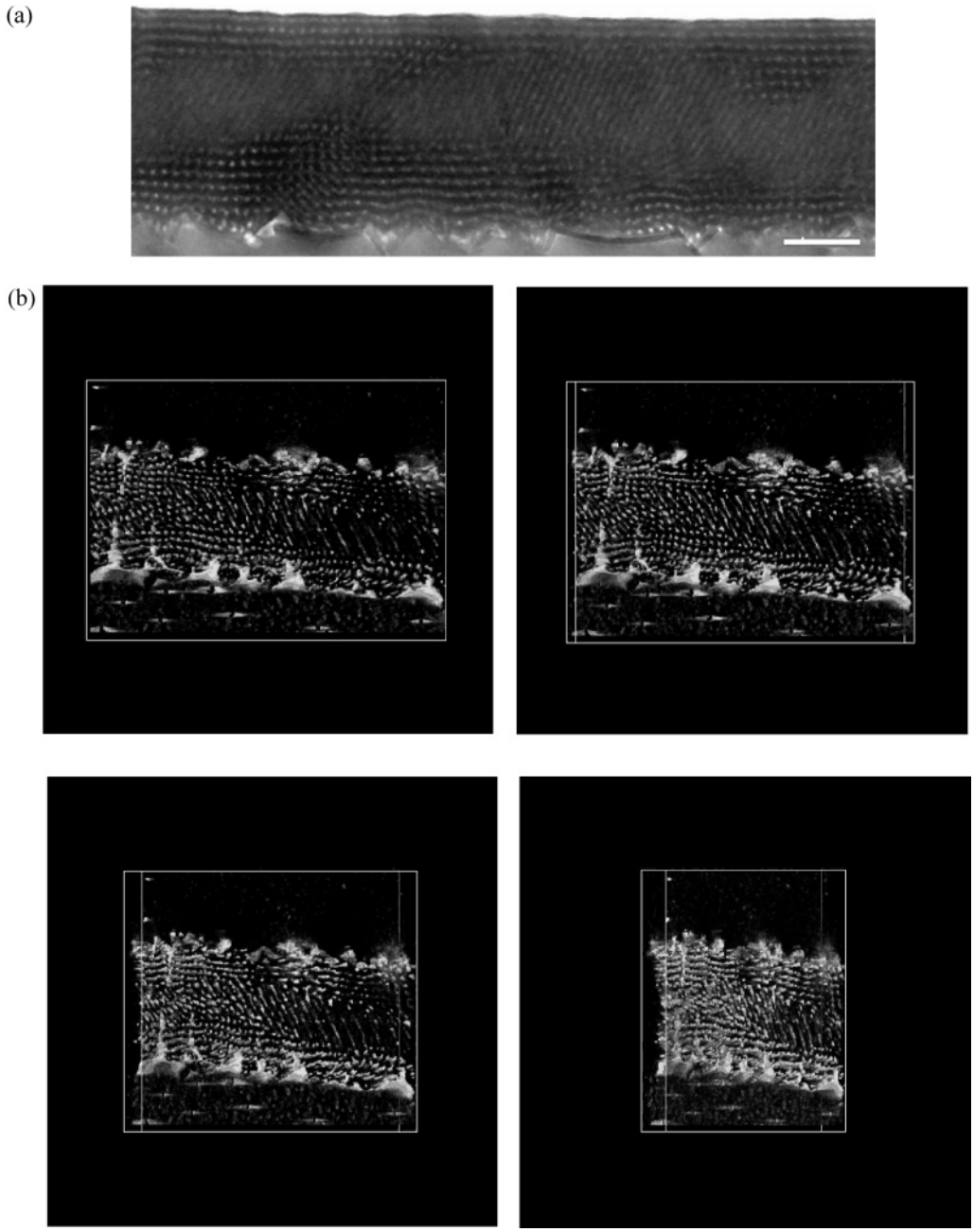

Figure 8. (a) Cross-sectional TEM images of a ~500 nm preannealed dPS-*b*-PMMA (47K) thin film after annealing under a ~40 V/μm electric field for 29 h. Scale bar: 200 nm. (b) A series of snapshots of PS-*b*-PMMA morphology (3-D TEM tomography of Figure 6a) viewing from different angles. The section was tilted from −73° to 57° with 1° increment. The box size is 288 nm × 288 nm × 77 nm. The top surface corresponds to the copolymer/substrate interface and the bottom to the copolymer/electrode interface. PMMA microdomains appear lighter color due to the lower electron density.

V/μm applied electric field for 9, 12, 16 h, respectively. The samples were identical except for the annealing time under the applied electric field. Cross sections were microtomed at 90 ± 2° with respect to the substrate, as shown in Figure 3a. After annealing under an applied electric field for 9 h, randomly oriented cylindrical PMMA microdomains are seen. Even with interfacial interactions, the cylindrical microdomains adjacent to the copolymer/substrate interfaces were not completely parallel to the interface, and the grain size of the cylindrical microdomains was very small. After annealing under an applied electric field for 12 h (Figure 3c), ellipsoid-shaped objects are seen with their long axes oriented in the direction of the applied field. Further annealing (16 h) leads to cylinders aligned along the field direction (Figure 3d).

Figure 3c is quite revealing in understanding the alignment process. In general, TEM images reflect the planar projection of the morphology, which gives rise to some ambiguity in interpretation. The TEM image shown here can be explained by having either a fraction of the cylinders oriented normal to the film surface being tilted out of the imaging plane or by ellipsoid-shaped microdomains. 3-D TEM tomography, a powerful technique to study morphologies, was used to further clarify the electric field alignment process.[41,42] Figure 3e shows a snapshot of the 3-D tomography of the film in Figure 3c. As can be seen, the cylindrical microdomains orient in the direction of the field lines, i.e., normal to the film surface, but alignment is not complete, as indicated by the inclination angle of the microdomains with respect to the field direction. With time, a further rotation of

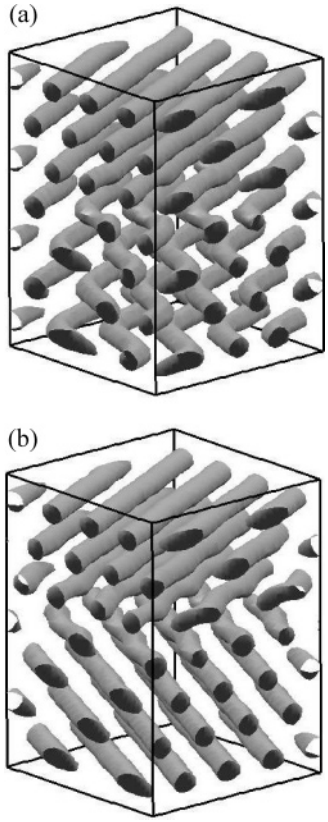

Figure 9. DSCF simulation snapshots of the asymmetric block copolymer melt prior to applying an electric field: (a) microstructure after 5000 time steps (TMS); (b) microstructure after an additional 5000 TMS of phase separation with preshearing at dimensionless shear rate 0.001. Here and further the images show isodensity surfaces (50% of the maximum concentration) of the minority block. The electrodes are located at the top and bottom of the boxes and are not shown in the images.

the microdomains leads to an alignment of the microdomains in the applied field direction. This image, along with those obtained at other observation angles, shows that the cylindrical microdomains are not interconnected and that they span the entire film. It is also apparent that the electric field has fully overcome interfacial interactions that tend to orient the microdomains parallel to the interfaces.

Combining the SANS and TEM results, a mechanism for the alignment of the copolymer microdomains from a poorly ordered starting point can be proposed. Initially, the copolymers form cylindrical microdomains with the orientations biased by both the interfacial interactions and applied electric field. With time, the electric field slowly distorts and rearranges individual cylindrical microdomains in the applied field direction. With time, the distorted microdomains combine and form cylindrical microdomains oriented in the direction of the applied field. This orientation mechanism in thin films takes many hours.

Initial State: Ordered State (Preannealed). For a copolymer having ordered microdomains oriented initially parallel to the film surface (normal to the field direction), Thurn-Albrecht et al. showed that the applied field leads to an instability that enables large grains to be broken up into smaller grains. However, the wavelength of this instability was not determined, and the details of the alignment process were not immediately clear. Here, we attempted to address these questions by investigating the electric field alignment of cylindrical microdomains in thin films ($<1\ \mu$m) that have been preannealed, which, due to preferential interaction of the blocks with the sample interfaces, causes the microdomains to be oriented parallel to the surface of the film.

As stated previously, the microdomain alignment is a competition between interfacial interactions and the applied electric field. Previous studies have shown that the parallel orientation of the microdomains persisted into the film over a distance that depends on the strength of the interfacial interactions.[43] Figure 4a−c shows the SANS patterns of ∼200, ∼300, and ∼500 nm dPS-*b*-PMMA (47K) films annealed at 170 °C for 72 h. When the film is thinner than the critical film thickness, the interfacial interaction orients the cylindrical microdomains throughout the film and a four-spot scattering pattern is seen (Figure 4a,b). When the film thickness is larger than this critical thickness, cylindrical microdomains in the interior of the film assume random orientations, giving rise to the ring pattern in Figure 4c. For the ∼500 nm annealed dPS-*b*-PMMA (47K) films, the cylindrical microdomains orient parallel to the surface in the vicinity of the copolymer/substrate interface and are randomly oriented in the center of the film.

Shown in Figure 5a−c are the SANS patterns for the ∼300 nm film in Figure 4b after annealing under an electric field (∼40 V/μm) for 3, 7, and 29 h, respectively. A four-spot scattering pattern is seen, but the shape of the pattern has changed dramatically. The spots are significantly smeared out, and the pattern appears elliptical in shape. This may arise from a deformation of the cylindrical microdomains in the direction of the applied field. Figure 6a shows a typical cross-sectional TEM image after annealing the film under a ∼40 V/μm electric field for 29 h (the same sample as that in Figure 5c). Within the field of view (∼5.5 μm in length), only spherical objects are seen. Considering the small grain size typically obtained with annealed block copolymer thin films, it is highly unlikely that the spherical objects are edge-on cylindrical microdomains. Thus, one is forced to conclude that the electric field enhances fluctuations with a characteristic wavelength D along the cylindrical microdomains. With time, the fluctuations grow in amplitude and, eventually, the cylindrical microdomains break up into spherical microdomains. Figure 6b shows a series of 3-D TEM tomographic images that further support the 2-D TEM observations. Fluctuations having a characteristic period along the cylindrical microdomains are clearly evident.

There are striking similarities between Figure 6a and the TEM images of the order−order transition (OOT) shown by Lodge et al.[30] and Hashimoto et al.,[44] which suggests that the electric-field-induced cylinder-to-sphere transition is very similar to the thermoreversible OOT.[29−32] The data shown here suggest that the (100) plane of the hexagonally packed cylinders oriented parallel to the film surface transforms into the (110) plane of body-centered-cubic (bcc) packed spheres. The intermediate state of spherical microdomains, however, is not stable, and eventually the spherical domains deform into ellipsoids.[45] Figure 6c shows an enlarged TEM image where the deformed spheres are clearly evident. Interestingly, the spheres do not deform parallel to the applied electric field direction but instead appear to be tilted at an angle. With time these distorted spherical microdomains interconnect along the ⟨111⟩

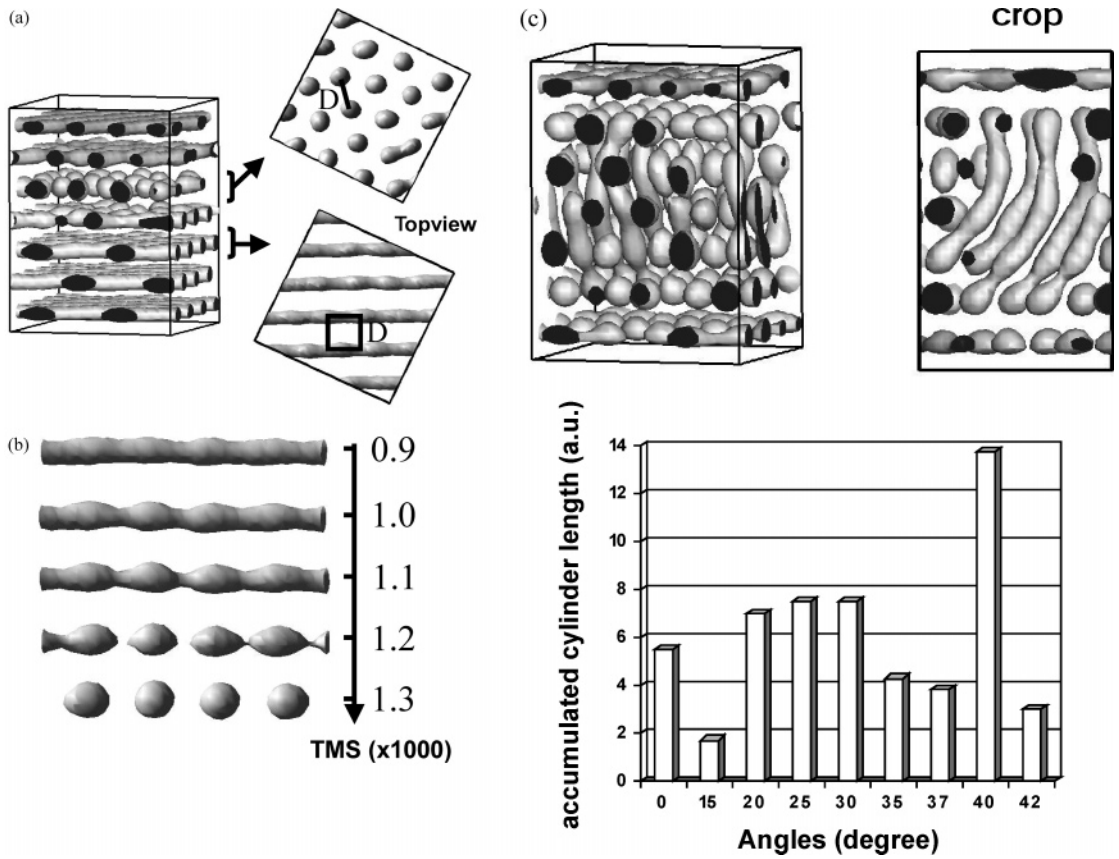

Figure 10. (a) DSCF simulation snapshots of the microstructure after 900 TMS of applying an electric field: onset of breakup to spheres. The electric field parameter is $\tilde{\alpha} = 0.05$. Separate pictures show details of the third and fifth layer, in which D is the cylinder−cylinder distance. (b) DSCF simulation snapshots of the side view of an individual cylinder in time elapsed after the electric field was applied (time steps, TMS). The cylinder is taken from the third layer from the bottom electrode. (c) DSCF simulation snapshots of the microstructure after 1300 TMS of applying an electric field. The crop image (right) shows only a part of the box on the left side, focusing on details of merging of the spheres into new cylinders. The histogram shows the distribution of tilt angles with respect to the electric field direction. The angles have been calculated from 2D slices through the long axis of cylindrical domains in the 3D structure; different slice direction in the $x-y$ plane have contributed equally.

direction of the body-centered-cubic packed spheres, producing cylinders with their long axis oriented in this direction.[45] Such a morphology of cylinders tilted with respect to the field direction is not energetically favorable, and the cylinders should reorient along the field direction with further annealing under the applied electric field. This process is very slow and was not observed experimentally even after annealing the thin films for 48 h.

The late stage of alignment was studied using a thicker film (∼500 nm), where after annealing the cylindrical microdomains are parallel to the surface at the copolymer/substrate interface and randomly oriented in the center of the film. Figure 7a shows the SANS pattern after annealing the ∼500 nm film (Figure 4a) under an electric field (∼40 V/μm) for 3 h. SANS patterns were observed that were similar to those of the ∼300 nm thick film, indicating the applied electric field deformed the cylindrical microdomains in a similar manner. The integrated peak intensity as a function of azimuthal angle is shown in Figure 7e. The plots are shifted vertically for clarity. After annealing for 7 h under an applied electric field, the scattering intensity increased for the reflections at ∼38° and ∼217° with a full width at half-maximum (fwhm) of 33°. The position of the maxima shifted to ∼45° and 222° (fwhm of ∼20°) and intensified with further annealing for 14 and 29 h, as shown in Figure 7c,d. Even after annealing under an applied electric field for up to 29 h, the cylindrical microdomains are not perfectly normal to the surface but are inclined at an angle of ∼45° with respect to the applied field direction. Compared to films beginning in a disordered state (as cast), the reorientation discussed here is a much slower process.

Figure 8a shows a cross-sectional TEM image of the film after annealing under a ∼40 V/μm electric field for 29 h (the same sample as that in Figure 7d). In the center of the film, where interfacial interaction effects are not important, the cylinders orient along the field direction at some tilt angle. At the copolymer/substrate interface, spherical microdomains are seen, as opposed to cylinders lying parallel to the interface. This is quite similar to the results for the thinner films shown previously. Figure 8b shows a series of tomographic images at different rotation angles of the film. In the center of the film, the cylindrical microdomains are aligned in the direction of the applied field, i.e., normal to the substrate. Adjacent to both interfaces, spherical-like microdomains that propagate several layers into the sample are seen. It can also be seen that the spherical microdomains are distorted in the direction of the applied field. The results further support the argument that the cylindrical microdomains break up into spherical microdomains under influence of the applied field. Subsequently, the spherical domains distort into ellipsoidal domains and then cylinders re-form, oriented at some angle with respect to the applied field. Subsequently, the cylinders rotate into the direction of the

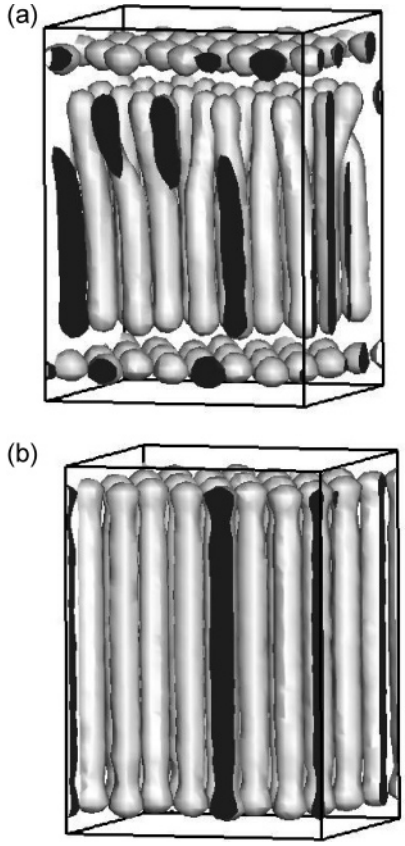

Figure 11. DSCF simulation snapshots of microstructures after 10 000 TMS of applying an electric field. (a) Final morphology and (b) final morphology in the case of higher E_0 ($\tilde{\alpha} = 0.1$).

applied field. The initial orientation of the cylindrical microdomains may have two origins. First, there is a simple geometric argument that the extent to which the spherical domains would have to deform and so as to merge into cylinders along the ⟨111⟩ plane is significantly less than if this occurred along the ⟨001⟩. In terms of interfacial energies, therefore, this would be more favorable. Second, if impurities within the copolymer caused the formation of microscopic dipoles in the microdomains (spherical microdomains), with excess charge (positive and negative charges located at the poles of the spherical microdomains), then the distance between poles of opposite charge is much shorter along the ⟨111⟩ than along the ⟨001⟩ . Consequently, electrostatics would favor a joining of the cylinders along this direction also. However, these are only speculative at this point and are being investigated further.

Simulations (Ordered Initial State). Similar details of the realignment process are seen in computer simulations based on dynamic self-consistent-field theory. All simulations start with a homogeneous diblock mixture at time step TMS = 0. Simulations indicate that the microphase separation begins at the wall surfaces and propagates into the bulk of the film. After 5000 time steps of simulation without applying an electric field, we obtain a sample (shown in Figure 9a) where preferential interactions have orientated the cylindrical microdomains parallel to the surface. Following the procedure used for lamellar systems,[46] the sample was initially presheared to achieve a better alignment of the cylinders (Figure 9b).

Application of an electric field normal to the cylinder axes destabilizes the cylindrical morphology (Figure 10a). The cylinders develop undulations along their axes with a characteristic wavelength equal to the distance D between cylinders. The undulations grow, as shown in Figure 10b, and eventually lead to the breakage of cylinders into spheres. As seen in Figure 10b, this process occurs rapidly (∼400 TMS), beginning in the middle of the film, where there are many grain boundaries (Figure 10a). As time proceeds, the spheres elongate into ellipsoids and merge with their neighbors (Figure 10c). This process also starts in the middle of the film and proceeds toward the electrodes. The newly forming and short cylinders often align in a direction that is not along the electric field direction but, similar to the experimental observations, show a tilt. As seen from the histogram in Figure 10c, the distribution of tilt angles has a maximum at ∼40°. It should be noted that the precise origin of the tilt observed in the simulations is not known, and it is difficult to draw any conclusions based on the similarities with the experiment. The initial stage of merging into short cylinders is comparable in time with the breakage of cylinders into spheres (about 500 TMS). The formation of well-aligned cylinders takes much longer. Figure 11a shows the final stage (after 10^4 TMS) of applying the electric field. All cylinders are almost perfectly aligned in the direction of the applied field. Close inspection shows that there are some dislocations, which are not too costly energetically. Adjacent to the interface of each electrode, there is one layer of spheres as a result of the competition of the applied electric and surface fields. The dislocations are very long-lived defects in the structure but can be eliminated with higher electric field strengths (Figure 11b). At this field strength all spheres merge and form a perfect single grain of hexagonally packed cylinders.

Conclusions

The electric field alignment of cylindrical microdomains in thin films of asymmetric diblock copolymers was investigated beginning from two different initial states, poorly ordered and well-ordered, with cylinders oriented parallel to the substrate. From the poorly ordered state, the microdomains orient under the influences of both interfacial interactions and the applied electric field. The interfacial interactions orient the microdomains parallel to the surface, whereas the applied field orients the microdomains along the field direction. Starting from a poorly ordered state, the copolymer microphase separates into very small grains. The energetic barrier to orient the cylindrical microdomains at the copolymer/substrate interface is not very high. The cylindrical microdomains are seen to rearrange locally and align along the field direction. For thin films beginning with cylinders parallel to the surface, the applied electric field enhances periodic fluctuations along the cylindrical microdomains with a wavelength comparable to D, the center-to-center distance of the cylindrical microdomains. These fluctuations increase in amplitude, causing the cylindrical microdomains to break up into spherical microdomains. TEM images suggest that this electric-field-induced sphere-to-cylinder transition is similar to thermoreversible cylinder-to-sphere order−order transition. With time, the spheres deform into ellipsoids that reconnect into cylindrical microdomains oriented at ∼45° with respect to the applied field direction. Further annealing aligns these tilted cylinders along the applied field direction. Results from simulations are consistent with these observations.

Acknowledgment. This work was funded in part by Department of Energy, Office of Science (DEFG02-96ER45612), and National Science Foundation-supported Material Research Science and Engineering Center (MRSEC) at the University of Massachusetts, Amherst (DMR-0213695). We acknowledge the support of the National Institute of Standards and Technology, U.S. Department of Commerce, in providing the neutron research facilities used in this work. This work utilized facilities supported in part by the National Science Foundation under Agreement DMR-9986442. H.J. is grateful to NEDO for supporting part of this study through a Japanese National Project "Nano Structure Polymer Project" by the Ministry of Economy, Trade and Industry. G.J.A.S. and K.S.L. acknowledge Stichting Nationale Computerfaciliteiten (NCF, Amsterdam) for providing computer time.We thank Dongseok Shin and James D. Sievert for assisting with SANS experiments. We also thank H. Nishioka for obtaining 3-D TEM pictures. The authors also thank Michael Schick (University of Washington), David Andelmann (University of Tel Aviv), and Yaov Tsori (Beer-Sheva University) for critical comments on this work.

References and Notes

(1) Park, M.; Harrison, C.; Chaikin, P. M.; Register, R. A.; Adamson, D. *Science* **1997**, *276*, 1401.
(2) Huang, E.; Rockford, L.; Russell, T. P.; Hawker, C. J. *Nature (London)* **1998**, *395*, 757.
(3) Thurn-Albrecht, T.; Schotter, J.; Kastle, C. A.; Emley, N.; Shibauchi, T.; Krusin-Elbaum, L.; Guarini, K.; Black, C. T.; Tuominen, M. T.; Russell, T. P. *Science* **2000**, *290*, 2126.
(4) Fredrickson, G. H. *Macromolecules* **1987**, *20*, 2535.
(5) Karim, A.; Singh, N.; Sikka, M.; Bates, F. S. *J. Chem. Phys.* **1994**, *100*, 1620.
(6) Mansky, P.; Russell, T. P.; Hawker, C. J.; Mays, J.; Cook, D. C.; Satija, S. K. *Phys. Rev. Lett.* **1997**, *79*, 237.
(7) Anastasiadis, S. H.; Russell, T. P.; Satija, S. K.; Majkrzak, C. F. *Phys. Rev. Lett.* **1989**, *62*, 1852.
(8) Amundson, K.; Helfand, E.; Davis, D. D.; Quan, X.; Patel, S. S.; Smith, S. D. *Macromolecules* **1991**, *24*, 6546.
(9) Morkved, T. L.; Lu, M.; Urbas, A. M.; Ehrichs, E. E.; Jaeger, H. M.; Mansky, P.; Russell, T. P. *Science* **1996**, *273*, 931.
(10) Thurn-Albrecht, T.; DeRouchey, J.; Russell, T. P.; Jaeger, H. M. *Macromolecules* **2000**, *33*, 3250.
(11) Boker, A.; Elbs, H.; Hansel, H.; Knoll, A.; Ludwigs, S.; Zettl, H.; Zvelindovsky, A. V.; Sevink, G. J. A.; Urban, V.; Abetz, V.; Muller, A. H. E.; Krausch, G. *Macromolecules* **2003**, *36*, 8078.
(12) Thurn-Albrecht, T.; Steiner, R.; DeRouchey, J.; Stafford, C. M.; Huang, E.; Bal, M.; Tuominen, M.; Hawker, C. J.; Russell, T. P. *Adv. Mater.* **2000**, *12*, 1138.
(13) Xu, T.; Kim, H. C.; DeRouchey, J.; Seney, C.; Levesque, C.; Martin, P.; Stafford, C. M.; Russell, T. P. *Polymer* **2001**, *42*, 9091.
(14) Amundson, K.; Helfand, E.; Quan, X.; Smith, S. D. *Macromolecules* **1993**, *26*, 2698.
(15) Amundson, K.; Helfand, E.; Quan, X. N.; Hudson, S. D.; Smith, S. D. *Macromolecules* **1994**, *27*, 6559.
(16) Fukuda, J.; Onuki, A. *J. Phys. II* **1995**, *5*, 1107.
(17) Onuki, A.; Fukuda, J. *Macromolecules* **1995**, *28*, 8788.
(18) Pereira, G. G.; Williams, D. R. M. *Macromolecules* **1999**, *32*, 8115.
(19) Ashok, B.; Muthukumar, M.; Russell, T. P. *J. Chem. Phys.* **2001**, *115*, 1559.
(20) Boker, A.; Elbs, H.; Hansel, H.; Knoll, A.; Ludwigs, S.; Zettl, H.; Urban, V.; Abetz, V.; Muller, A. H. E.; Krausch, G. *Phys. Rev. Lett.* **2002**, *89*, 135502.
(21) Thurn-Albrecht, T.; DeRouchey, J.; Russell, T. P.; Kolb, R. *Macromolecules* **2002**, *35*, 8106.
(22) Tsori, Y.; Andelman, D. *Macromolecules* **2002**, *35*, 5161.
(23) Tsori, Y.; Tournilhac, F.; Andelman, D.; Leibler, L. *Phys. Rev. Lett.* **2003**, *90*, 145504.
(24) Tsori, Y.; Tournilhac, F.; Leibler, L. *Macromolecules* **2003**, *36*, 5873.
(25) Xu, T.; Hawker, C. J.; Russell, T. P. *Macromolecules* **2003**, *36*, 6178.
(26) Xu, T.; Goldbach, J. T.; Leiston-Belanger, J.; Russell, T. P. *Colloid Polym. Sci.* **2004**, *282*, 927.
(27) Xu, T.; Zhu, Y.; Gido, S. P.; Russell, T. P. *Macromolecules* **2004**, *37*, 2625.
(28) Zvelindovsky, A. V.; Sevink, G. J. A. *Phys. Rev. Lett.* **2003**, *90*, 049601.
(29) Ryu, C. Y.; Lodge, T. P. *Macromolecules* **1999**, *32*, 7190.
(30) Ryu, C. Y.; Vigild, M. E.; Lodge, T. P. *Phys. Rev. Lett.* **1998**, *81*, 5354.
(31) Kimishima, K.; Koga, T.; Hashimoto, T. *Macromolecules* **2000**, *33*, 968.
(32) Sakurai, S.; Hashimoto, T.; Fetters, L. J. *Macromolecules* **1996**, *29*, 740.
(33) Mansky, P.; Liu, Y.; Huang, E.; Russell, T. P.; Hawker, C. *Science* **1997**, *275*, 1458.
(34) Luther, P. K.; Lawrence, M. C.; Crowther, R. A. *Ultramicroscopy* 1988, *24*, 7.
(35) Radermacher, M. In *Weighted Back-Projection Methods In Electron Tomography;* Frank, J., Ed.; Plenum Press: New York, 1992; p 91.
(36) Zvelindovsky, A. V.; Sevink, G. J. A.; Fraaije J. G. E. M. In *Simulation Methods for Polymers*; Kotelyanskii, M. J., Theodorou, D. N., Eds.; Marcel Dekker: New York, 2004; Chapter 18, pp 575−597.
(37) van Vlimmeren, B. A. C.; Maurits, N. M.; Zvelindovsky, A. V.; Sevink, G. J. A.; Fraaije, J. G. E. M. *Macromolecules* **1999**, *32*, 646.
(38) Landau, L. D.; Lifshitz, E. M. *Electrodynamics of Continuous Media;* Pergamon: Oxford, 1960; Section 10.
(39) Sevink, G. J. A.; Zvelindovsky, A. V.; van Vlimmeren, B. A. C.; Maurits, N. M.; Fraaije, J. G. E. M. *J. Chem. Phys.* **1999**, *109*, 2250.
(40) Pu, Y,; Rafailovich, M. H.; Sokolov, J.; Gersappe, D.; Peterson, T.; Wu, W.-L.; Schwarz, S. A. *Phys. Rev. Lett.* **2001**, *87*, 206101.
(41) Jinnai, H.; Ikehara, T.; Nishi, T. *Adv. Polym. Sci.* **2004**, *170*, 115.
(42) Jinnai, H.; Nishikawa, Y.; Spontak, R. J.; Smith, S. D.; Agard, D. A.; Hashimoto, T. *Phys. Rev. Lett.* 2000, *84*, 518.
(43) Xu, T.; Hawker, C. J.; Russell, T. P. *Macromolecules* **2005**, *38*, 2802.
(44) Sota, N.; Sakamoto, N.; Saijo, K.; Hashimoto, T. *Macromolecules* **2003**, *36*, 4534.
(45) Xu, T.; Zvelindovsky, A. V.; Sevink, G. J. A.; Gang, O.; Ocko, B.; Zhu, Y.; Gido, S. P.; Russell, T. P. *Macromolecules* **2004**, *37*, 6980.
(46) Zvelindovsky, A. V.; Sevink, G. J. A.; Vlimmeren, B. A. C. v.; Maurits, N. M.; Fraaije, J. G. E. M. *Phys. Rev. E* **1998**, *57*, R4879.

MA050521C